SFSA Cast in Steel 2025 – George Washington's Sword Technical Report

University of Tennessee Knoxville – Team Sword Washington

Team Members:
Davis Granger - Senior Undergraduate Student (Material Science and Engineering)
Nolan Lees - Senior Undergraduate Student (Material Science and Engineering)
Fabriana Prawiranata - Senior Undergraduate Student (Material Science and Engineering)
Daniel Rasmussen - Senior Undergraduate Student (Material Science and Engineering)
Jakob Scroggins - Senior Undergraduate Student (Material Science and Engineering)

Advisor:
Dustin Gilmer – Post-Doctoral Fellow at the UT-Oak Ridge Innovation Institute

Foundry Partners:
Magotteaux
Andritz

Executive summary

The Cast in Steel competition challenges students to use modern casting technologies and their knowledge of metallurgy to design and fabricate an object of historical, cultural, or practical relevance. This year, students were challenged to make a replica of one of George Washington's swords, which will undergo testing for durability and functionality. Washington owned several swords of many different varieties—including broadswords, epees, and cuttoes. The team from the University of Tennessee, Knoxville Department of Materials Science and Engineering, known as Team Sword Washington, has selected Washington's Bailey silver and ivory hilted cuttoe to replicate due to its bold colors and simplistic aesthetics. Team Sword Washington is advised by Dr. Dustin Gilmer, an assistant professor in the materials-science department, and has been fortunate enough to collaborate with many industry professionals and companies.

Prioritizing efficiency and playing to the strengths of its members, Team Sword Washington divided the material selection and design workload into two subgroups: one focused on alloy selection and the other focused on mold design. The alloy-selection team began by considering constraints likely to be imposed by the competition's performance testing. These included bending, wear resistance, and sharpness. These were translated into the following material properties, which were used to guide the material-selection process: elasticity, yield strength, and hardness. Because of the presence of voids inherent in cast materials, fracture toughness was added as an important material property. Optimization of these material properties, with consideration of alloy cast-ability, narrowed the team's choice material to 17-4 precipitation-hardenable stainless steel. To improve the hardness of this alloy, the team explored surface treatments—including carburizing, nitriding, nitrocarburizing, and Kolsterising.

Simultaneously, the mold-design team worked to create a faithful CAD model of the blade and mount replicates of it on a casting tree. Iterations of the casting-tree design were performed, maximizing efficiency and material use. The alloy selection was used to inform computational fluid dynamics (CFD) simulations that were translated into further design improvements that minimized turbulent flow and back-flow from the blade into the sprue. Recognizing that time and resources allowed only one cast, blades of varying thickness (and therefore, varying probability of success) were incorporated into the design. The final mold consisted of six blades of varying thicknesses mounted radially around a sprue.

The individual strengths and collaborative efforts of the members of Team Sword Washington culminated in the successful fabrication of a replica of Washington's Bailey silver and ivory hilted cuttoe. Due to time constraints, surface treatment was not carried out, but a plan to increase the blade's hardness is outlined in this report, and preliminary characterization is presented. Team Sword Washington submitted a cast sword, fit for Washington, weighing ~650 g with an overall length of 36 in., compliant with the Cast in Steel requirements.

1. SFSA and George Washington's sword

The Steel Founders' Society of America (SFSA) was founded in 1902 to represent and support the steel-casting industry in the US [1]. Since then, SFSA has been dedicated to advancing steel foundries through research, technological development, industry standards, and educational outreach. By promoting innovation and best practices, the organization plays a crucial role in ensuring the growth and sustainability of steel casting as a manufacturing sector.

One of SFSA's initiatives is the "Cast in Steel" competition, an annual event designed to engage university students in the art and science of steel casting. SFSA has created this competition to encourage students to learn about making steel products using the casting process and applying the latest technology available. This requires them to demonstrate both technical expertise and creative problem solving. Each year, the competition focuses on a different object; for example, the 2024 challenge involved creating a Halligan bar, a tool used by firefighters. Students must also submit a detailed technical report and a video explaining their design process and performance of their final product.

This year, students are challenged to create a functional replica of one of George Washington's swords. As a military leader and the first president of the US, Washington owned several swords that reflected both his status and the era's craftsmanship. One of his most well-known swords is the 1753 silver-hilted smallsword, which he carried during the French and Indian War [2]. This weapon exemplifies the refined design of 18th-century swords. Another significant piece in his collection is the 1767 silver-hilted smallsword, which is prominently featured in various portraits of Washington [2]. Additionally, Washington's battle sword, a Bailey silver and ivory-hilted cuttoe dating to around 1765, was later inherited by his nephew, Samuel T. Washington [2, 3]. In his will, Washington advised that the weapon should only be used for self-defense or in the protection of the nation [3]. These swords are preserved in institutions such as his estate, Mount Vernon, and the Smithsonian National Museum of American History.

Sword-making in the 18th century, including the methods used for George Washinton's swords, involved a combination of forging, grinding, and finishing techniques. Blacksmiths would begin by heating high-carbon steel or iron in a forge until it was malleable. The metal was then hammered into the rough shape of a blade. To achieve the desired strength and flexibility, the blade underwent repeated cycles of heating, hammering, and quenching in water or oil to harden the steel. After hardening, the blade was tempered by reheating it to a lower temperature, reducing brittleness while maintaining durability [4]. Swordsmiths would then grind and polish the blade to refine its shape and sharpen the cutting edge. The hilt, often made of silver or brass, was crafted separately through casting or forging and then attached to the tang of the blade [4]. Decorative elements, such as intricate engravings or wire-wrapped grips, were added to enhance the aesthetic appeal of the sword. This process resulted in weapons that were both effective in combat and symbols of status and prestige.

2. Material selection

To select an optimal material for a sword, we first considered what functions a sword must perform and what material properties map to those functions. A high-performance blade should be able to cut effectively, bend without breaking, and survive impact against other blades and objects. The ideal material properties for each of these functions, summarized in Table 1, are elaborated on throughout this section along with the screening process, and ultimately, CB7Cu-1, a casting variant of 17-4 stainless steel, is chosen.

Table 1. Translation of functions to material properties.

Function	**Material properties**
Cutting	• Hardness > 400 HV
Flexibility	• Low elastic modulus • High yield strength
Impact strength	• Fracture toughness > 52 MPa.m$^{0.5}$

2.1 Cutting

A blade's ability to cut is tied to its edge retention, where the premier influencing material attribute is hardness. The blade must be harder than the material it is attempting to cut through to maintain the integrity of the edge and prevent chipping or plastic deformation. For a high-performance blade, hardness values can range from 500-700 HV (50-60 HRC) [5]. This range is difficult to obtain from typical cast alloys, so for the purpose of this selection process, a lower threshold value of 400 HV was considered sufficiently hard with the intent to further increase hardness by surface treatment.

2.2 Flexibility

Flexibility influences the durability of a blade—as a more flexible blade is able to bend and rebound upon impact instead of breaking. A method of evaluating this property would be a bend test, as seen in Fig. 1, in which the tip of the sword is a fixed point and force is applied at the handle until the sword breaks or is plastically deformed. The deflection and force at failure for this scenario can be described by equations 1 and 2.

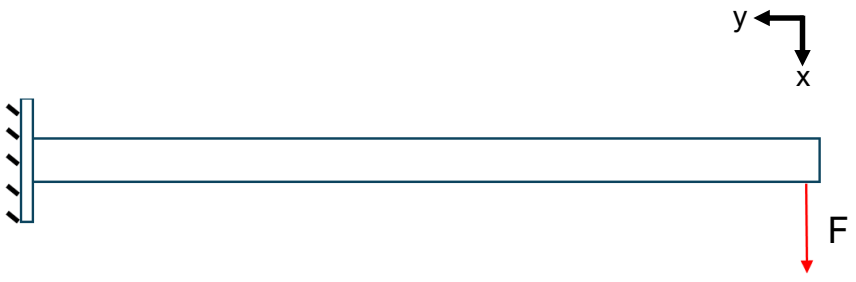

Figure 1. Free body diagram of bend test.

$$\delta = \frac{FL^2}{C_1 EI} \quad \text{eq. 1 [6]}$$

$$F_f = \frac{Z\sigma_Y}{L} \quad \text{eq. 2 [6]}$$

where δ is the deflection; F_f is the force at failure; F is the force applied; L is the length; E is the elastic modulus; σ_Y is the yield strength; and C_1, I, and Z are geometric constants. Further, by combining the two equations into equation 3, we can find the deflection at failure, δ_f. Based on this equation, in order to maximize δ_f, we desire a material with a high yield strength and a low elastic modulus.

$$\delta_f = \frac{Z\sigma_Y L}{C_1 EI} \quad \text{eq. 3}$$

2.3 Impact strength

The blade's durability is also related to the material's ability to prevent defect propagation and fracture upon impact, i.e. fracture toughness. To establish a lower threshold for this material property, we used the fracture toughness of 1095 steel, as it is a common material for knife blades. Thus, we consider materials with a fracture toughness of at least 52 MPa.m$^{0.5}$ as appropriate for this application [7].

2.4 Screening

The first materials-screening parameters ensured compliance with the bounds set by the competition—specifically, the material choice must be castable and an Fe-C alloy. These requirements were applied to a large candidate pool of various metals, as seen in Fig. 2, and surviving candidates were then further screened based on mechanical properties.

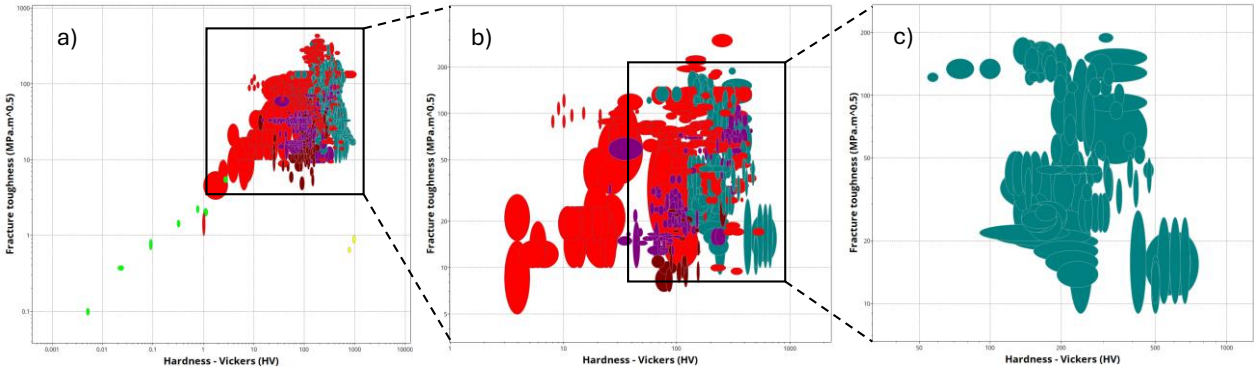

Figure 2. Candidate pool of a) all metals, b) castable metals, and c) castable Fe-C alloys [7].

Candidates were evaluated based on fracture toughness and hardness to determine if the material has sufficient cutting ability and impact strength. When the constraints for these properties, described in Table 1, are applied to the pool of candidates, two groups of materials, shown in Fig. 3, remain as viable options. The first group of materials consists of Cr-Ni-Cu alloyed

martensitic stainless steels which vary by heat treatment and by alloyed-metal composition. The second group contains different grades of austempered ductile iron (ADI).

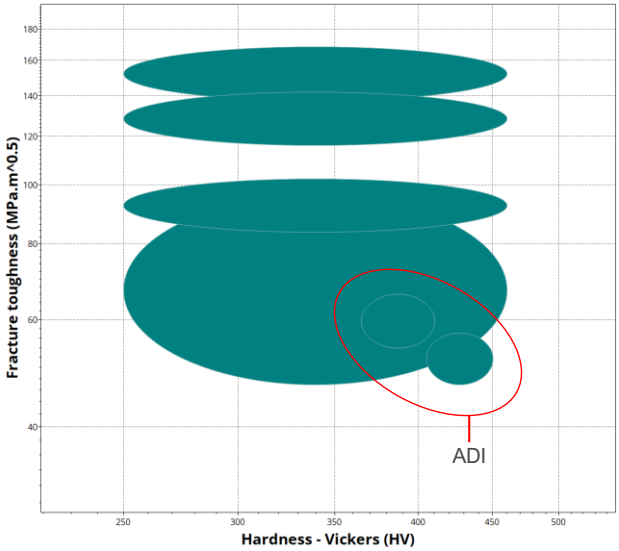

Figure 3. Ashby plot of fracture toughness vs. hardness [7].

The last round of screening identifies candidates with high flexibility. A flexible material must have both a low elastic modulus to allow for elasticity and a high yield strength to prevent deformation. As seen in equation 4, an index balancing these two properties was used to determine the suitability of the candidates.

$$M = \frac{\sigma_Y}{E} \qquad \text{eq. 4 [6]}$$

where M is the index, σ_Y is yield strength, and E is elastic modulus. A selection line was then derived from this index and adjusted on the Ashby chart in Fig. 4 to exclude materials with a low index. This leaves three surviving candidates: 17-4 H900 martensitic stainless steel (SS), grade 1200 ADI, and grade 1400 ADI.

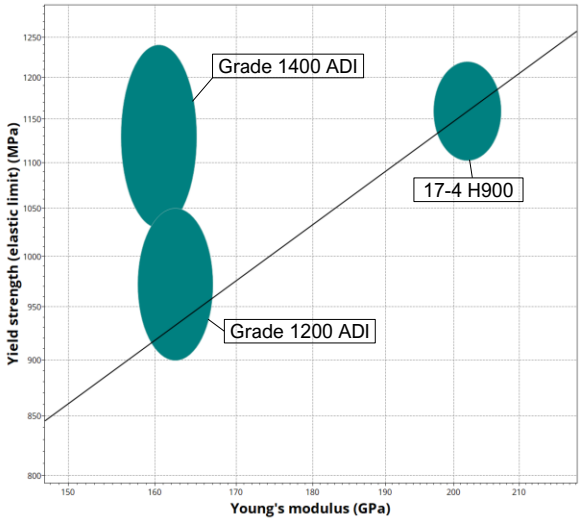

Figure 4. Ashby plot of yield strength vs. Young's modulus [7].

2.5 Selection

The performance of the sword hinges on the hardness, fracture toughness (K_{IC}), yield strength (σ_Y), and elasticity (E) of the chosen material. Thus, we must compare these properties across all three candidates to find an ideal material. Table 2 summarizes the relevant mechanical properties of the candidate materials.

Table 2. Mechanical properties for all candidates [7].

Material	**Hardness (HV)**	**K_{IC} (MPa.m$^{0.5}$)**	**σ_Y (MPa)**	**E (GPa)**
ADI 1200	365-410	54-66	900-1050	158-167
ADI 1400	405-450	47-57	1030-1240	156-165
17-4 SS	250-460	47-96	1100-1220	197-207

We can see that 17-4 SS has the highest maximums for all properties, excluding yield strength, and even then, the alloy is second place by a small margin. Thus, 17-4 SS is clearly the superior alloy based on mechanical properties and is promising for producing a high-performance cast blade.

Additionally, the wide range in hardness values demonstrates the tunability of the alloy. 17-4 SS can be strengthened through precipitation hardening and by varying parameters such as aging temperature and time, we can have a high degree of control over the microstructure and resulting properties. This hardening is made possible primarily through three constituent elements: Ni, Cu, and Nb. Ni influences hardenability by enhancing the steel's ability to form martensite during cooling. It stabilizes austenite by lowering the critical cooling rate required to form martensite [8]. By inhibiting ferrite and pearlite formation, the austenite-to-martensite transformation can occur over a broad temperature range [8]. After martensite formation, aging treatment forms Cu-rich, coherent precipitates in the BCC martensite matrix [9]. This occurs in distinct stages: diffusion of atoms together to form precipitates, growth of the precipitates, and coarsening [9]. These precipitates serve as inhibitors of dislocation motion, increasing strength and hardness.

The mechanical properties and tunability of 17-4 SS make it the ideal choice for casting of a blade. To improve manufacturability, we will be using the casting variant of the alloy, CB7Cu-1.

3. Sword design and simulation

In addition to selecting a material, the sword must be designed taking into consideration structural integrity and historical references. We utilized tools including computer aided design (CAD) and finite element analysis (FEA) in pursuit of this.

3.1 CAD sword model

George Washington's Bailey silver and ivory cuttoe, pictured in Fig. 5a, is known for its historical significance as the sword that the artist Leutze depicts in his famous "Washington Crossing the Delaware" painting. It is known also for its intricate design and served as the template for this project, with its 30-in. (76 cm) blade length and complex hilt and handle design. To create a parametric model of the sword, first, a high-quality image of the blade was sourced from the Smithsonian website [3]. This image was then imported into SolidWorks CAD software and scaled

to match the dimensions of the sword. From this image, the base sketch of the sword was created as seen in Fig. 5b. Special care was taken to create a parametric model of the sword from this base sketch. A parametric model is advantageous for this project because it allows easy adjustments to critical dimensions—such as blade curvature, length, and thickness. This ensured any modifications automatically propagated though the design and maintains accuracy and consistency while saving time and effort. The curve, overall length, and thickness of the blade were critical features that required meticulous adjustments to align with the sword's original proportions. Determining the thickness proved to be a challenge since the blade needed to be thick enough to prevent issues when casting but thin enough to remain faithful to the original design. Techniques such as lofting for smooth transitions, extrusions for flat sections, and spline tools for matching the curve were used to recreate the geometry of the blade and handle. These efforts resulted in the model seen in Fig. 5c which takes into consideration both historical accuracy and manufacturability.

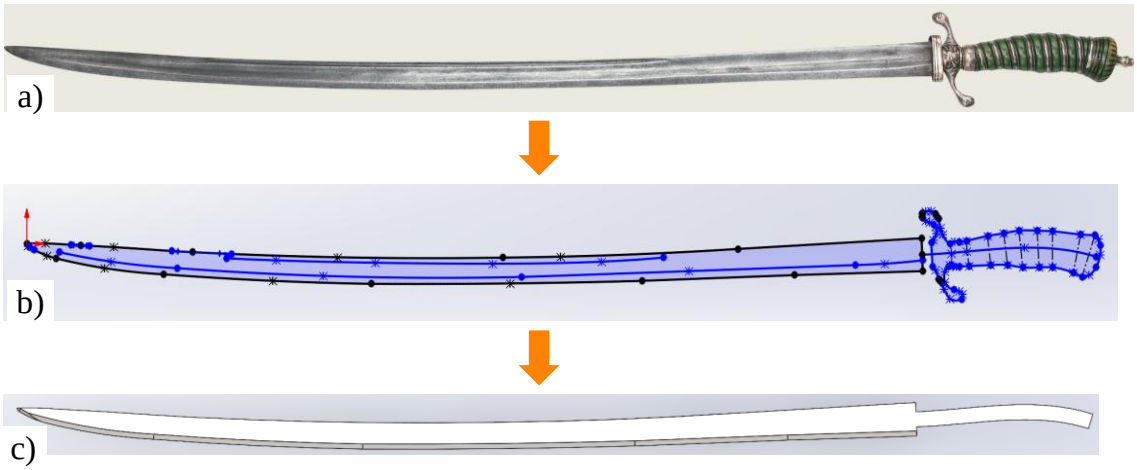

Figure 5. Design of the blade from a) historical reference to b) sketch to c) model [10].

3.2 FEA results

To ensure the structural integrity of the design, structural validation was carried out using the SolidWorks FEA software. The material tested was a cast alloy steel pulled from the SolidWorks database. For this simulation, the boundary conditions were set to mimic the bending test shown in Fig. 1. The load was applied on the handle, and the tip of the blade was fixed to simulate the jaws of a bench vise. Due to the possibility of uncertain porosity from the casting process, this simulation was treated with a certain level of understanding that real-world results would likely yield lower stress maximums. Thus, the main purpose of the simulation is to identify where stress concentrates in the blade and ensure a design flaw is not overlooked. The results of the simulation are shown in Fig. 6.

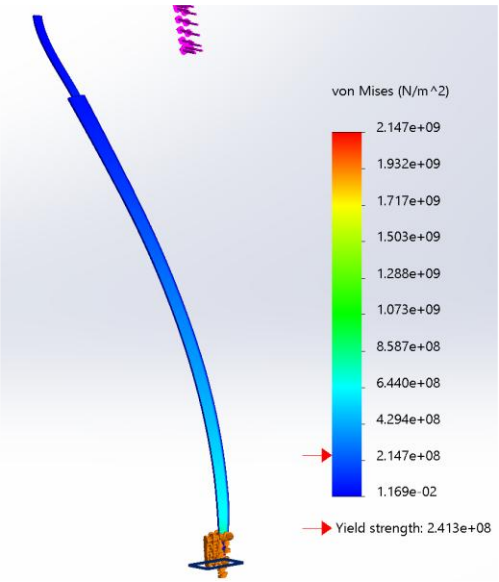

Figure 6. FEA results for bend test on the CAD sword model.

Based on the stress profile, we could ascertain that most of the load was localized at the tip of the blade where we would likely see failure during the real-world test. With that in mind, special attention can be paid to the grain-structure and porosity analysis of that section during post-processing of cast samples.

4. Mold design and simulation

Casting challenges, coupled with the intrinsic properties of the material, defined the mold-design requirements for this project. Issues such as material shrinkage, fluidity, and common casting concerns like gas entrapment are critical factors to consider during the casting process. Additionally, material properties like thermal conductivity, solidification ranges, and melt viscosity can significantly influence how the material flows and cools within the mold once poured. A mold that considers these factors and challenges must also produce at least six swords per cast to supply extra blades for testing and qualification.

4.1 Manufacturing

With the design requirements and resources available to the team in mind, the mold was designed to be printed using a binder jet printer. The binder jet printing technique allows for the highest quality mold surface, which in turn, creates more dimensionally accurate castings when compared to a lost-foam casting method. Furthermore, an advantage of using this process is the possibility of using water soluble polymers as the binder for the sand. The end objective of this would be to use high-pressure water to dissolve the sand mold and cool the swords much faster than a traditional cast mold which could take up to three days to cool to a safe temperature. An important consideration for this manufacturing method is the build envelope of the printer being smaller than the full length of the sword. This restriction created a need for the mold to be printed in two halves and attached afterwards.

4.2 Mold design process

Since the sword will be cast from 17-4 stainless steel, the molten flow properties and solidification behavior were carefully considered during the mold development stage. The initial prototype mold, seen in Fig. 7a, was kept simple and featured a parallel gate system. This design was eventually deemed inefficient due to its large footprint and inefficient pour ratio. Improving on this design yielded the second iteration, shown in Fig. 7b, which trades the parallel sword configuration for a radial configuration with horizontal gates coming out of the sprue. This iteration showed promise and was analyzed using Magotteaux's computational fluid dynamics (CFD) software MAGMA. Based on the CFD results, which are elaborated in the next section, changes were made to the design and resulted in the final version seen in Fig. 7c. The improved features include 45° angled gates connecting the sprue to the blade and the addition of a sprue cup.

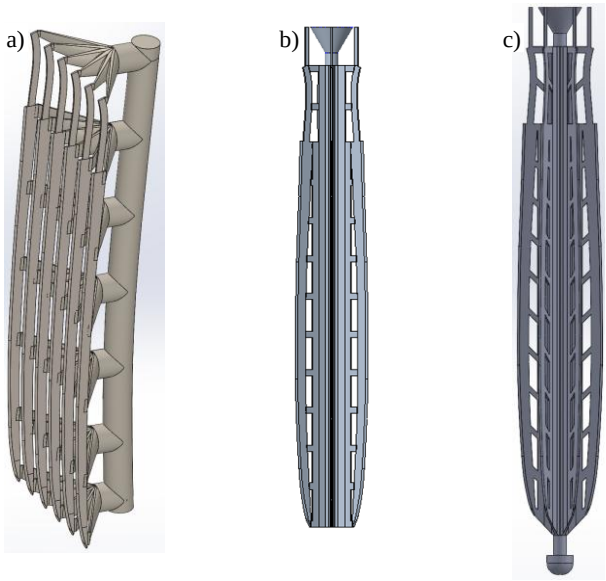

Figure 7. Iterations of the mold design: a) version 1, b) version 2, and c) version 3.

4.3 CFD simulation

CFD analysis on the mold is crucial to identifying potential problems during the casting process, especially when working within a time constraint that does not allow for continuous trial and error. The simulations were run using the parameters described in Table 3 and visualized how molten metal would flow through the mold. The analysis focused on key performance factors, such as temperature distribution and flow velocity to identify potential defects in the casting process.

Table 3. Simulation parameters used for CFD analysis of the mold.

Alloy	Cb7Cu1
Pouring temperature	1600°-1650°
Feeding Effectivity	35%
Net weight	2.19 kg
Gross weight	11.11 kg
Yield	19.68%
Pouring time	4.59 s

Fig. 8 shows the results for the solidification analysis and cooling of the mold over time. We can see that the molten metal cools as expected from the outside of the blade first and then towards the sprue. To further ensure proper solidification and prevent shrinkage defects, the risers in the final version were thickened. One concern found in this simulation is that the metal approaches the range of solidification temperatures of the alloy as it reaches the tang. The metal cools significantly as it travels from the tip to the tang, and premature solidification of the upper gates may cause incomplete filling of the mold. One way to address this issue would be to shorten the length of the sword; however, the original length must be maintained to ensure historical accuracy.

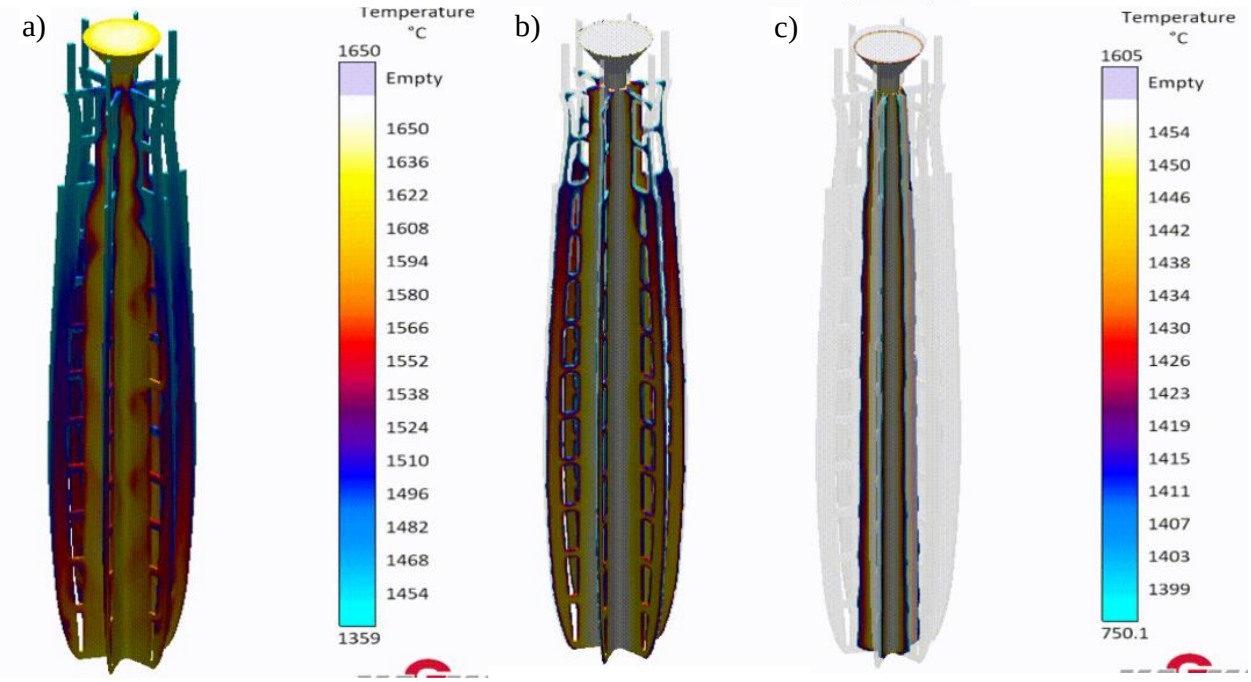

Figure 8. Temperature profile of the mold a) immediately after filled, b) 10 s after filled and c) 20 s after filled.

Flow velocity is another factor that contributes to the solidification of the sword. As seen in Fig. 9, the high velocity of the flow correlates to porosity probability as determined by the simulation. The flow direction presents an additional problem as the molten metal flows backwards into the main sprue cavity which is indicative of cold-shut behavior.

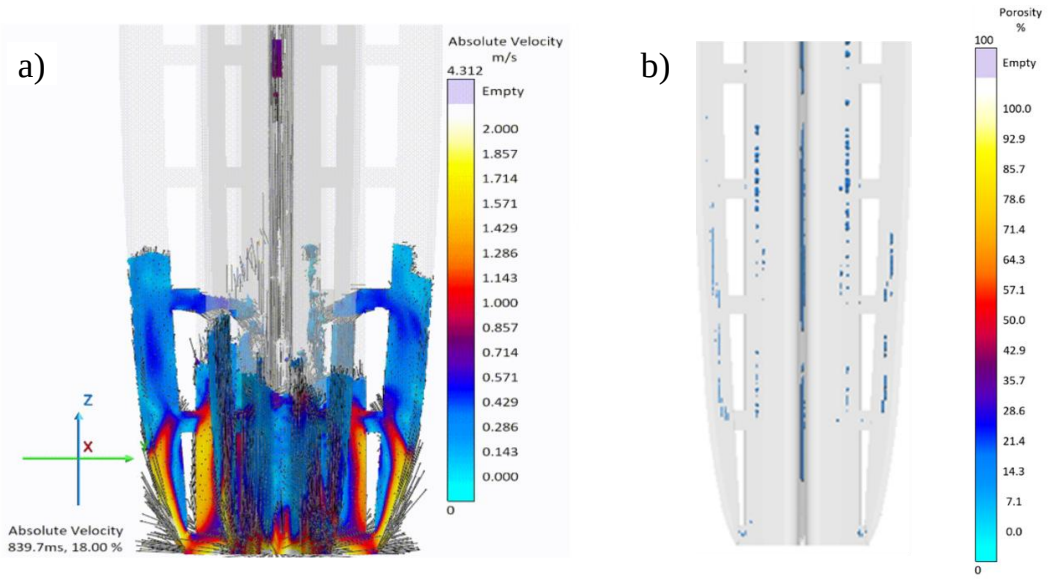

Figure 9. CFD results for a) velocity simulation and b) porosity simulation.

To address these issues, version 3 of the mold was extended on the bottom section to allow for the initial pour from the molten metal to be contained in a cup that would capture stray droplets and splashes from reaching the sword body. This iteration included strategically placed gates angled at 45° to direct the molten metal smoothly into the cavity and avoid sharp turns that could disrupt flow. The mold was re-simulated with these changes with the results shown in Fig. 10.

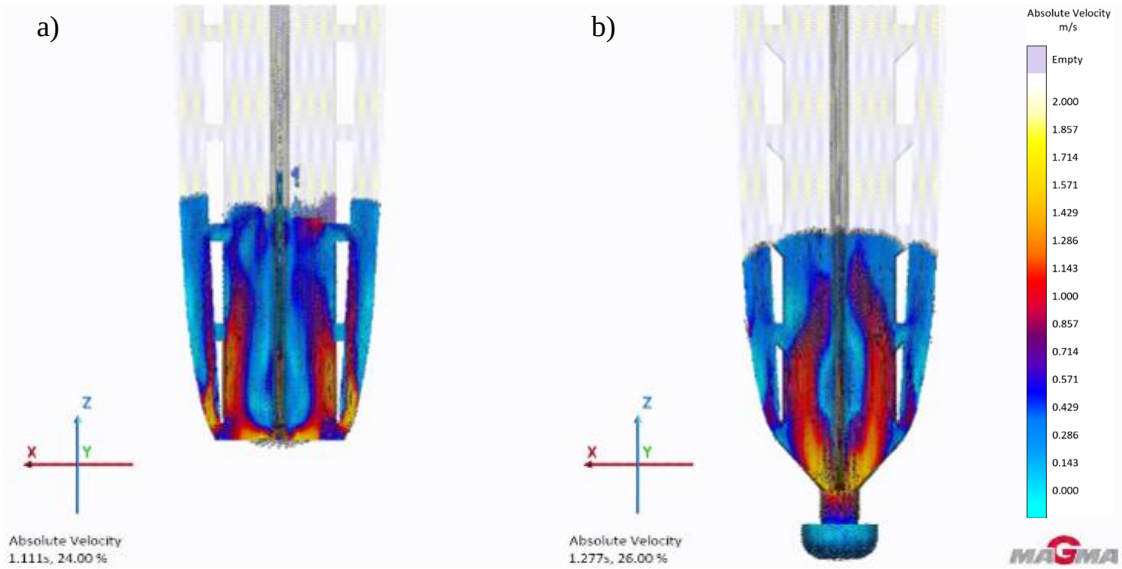

Figure 10. Flow velocity through the a) version 2 mold and b) version 3 mold.

As seen in Fig. 10, the CFD simulation of the third iteration of the mold design suggested that the change in gate angle and addition of sprue cup had an impact on the filling rate of the casting. In version 2, the blade cavity filled first and backfilled into the sprue, which is detrimental to the success rate of the mold by creating the chance for cold shuts to occur. In version 3 of the mold,

the sprue fills first and feeds the blade cavity. This is beneficial to the casting because more heat is stored in the sprue and is less likely to create opportunities for cold shut formation.

4.4 Final mold design

The final mold design, seen in Fig. 11, was decided using the best-performing CFD model. To create a shape using additive manufacturing, the positive geometry from the CFD model was subtracted from a hexagonal block of material, creating a hollow mold of the blade casting tree inside a printable shape. To maximize the chances of a successful pour with no cold shuts or defects, multiple blade thicknesses and profiles were added to the casting. Two of the blades were 0.125 in. thick, two were 0.250 in. thick, and the last two were 0.375 in. thick, with each pair having an edged version and non-edged rectangular version. Because the process of binder jet printing requires non-utilized sand to be removed from the part, the mold had to be designed to ensure the part could be depowdered. With this design consideration in mind, the mold was split perpendicular to the pouring direction, and locating pins were added to ensure blade lineup. Additionally, to prevent molten metal from escaping from the mold halves, a 45° chamfer was added to the split surface to prevent any metal from escaping.

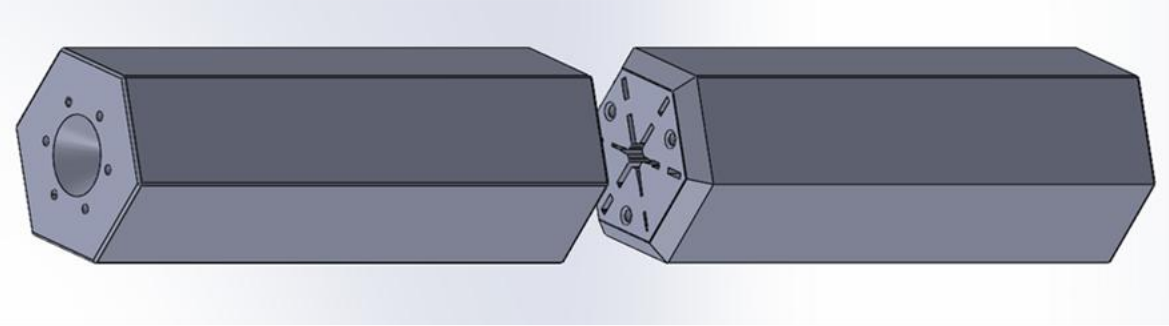

Figure 11. Final mold design that was printed.

5. Cross guard and handle model

Team Sword Washington took two design approaches to the cross guard and handle: one where the sword's handle, cross guard, and pommel are separate components and another where they are a single component. For both designs, the components are designed in halves to completely house the tang. The cross guard and handle was modeled in the same fashion as the blade, where an image of the blade was imported into SolidWorks and traced to retain the dimensional accuracy of the real item.

5.1 Separate-components design

The first handle design consisted of the grip as a separate component that would be cast around a scaffold containing the cross guard and pommel, as shown in Fig. 12. The grip would be cast from epoxy and the scaffolding made by 3D printing 316L stainless steel by laser powder bed fusion (LPBF) to ensure precision and preservation of the intricate details featured in the design. The two components would then be secured with pins and epoxy and the housing for the pins grinded flush to the grip.

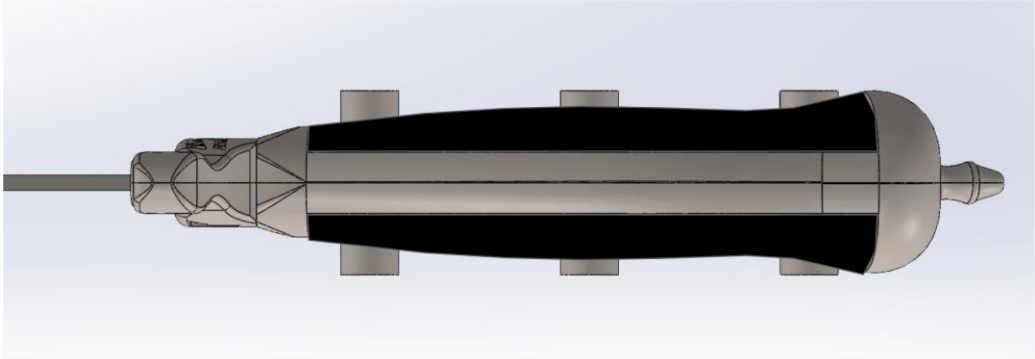

Figure 12. CAD model of the separate component design.

5.2 Single-component design

The second design of the handle, cross guard, and pommel combined these three pieces into a single component, as shown in Fig. 13. It features small holes where pins would go to secure both halves of the component with the tang in between. The simpler design allows for the structure to be sand cast with lower risks of complications. Additionally, it expands the materials available during manufacturing. With 3D printing we are limited to 316L stainless steel, but casting opens the door to all the materials we are able to melt and pour in the UTK lab spaces including, Cu, Sn, and Al.

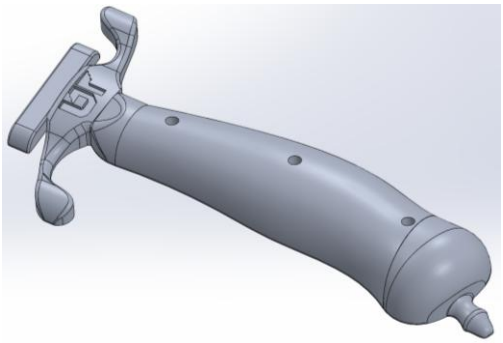

Figure 13. CAD model of the single-component design.

6. Fabrication

With models created for all the different parts of the sword, we then proceeded with manufacturing. This includes casting the mold and creating the cross guard, handle, and pommel. To achieve this, we coordinated with our industry contacts to print the mold for the blades and cast. At the same time, we explored our options for fabricating the handle with the resources available at UTK including 3D printing and sand casting.

6.1 Casting mold

Once the mold was printed at Mathews Additive Technologies, casting took place at Andritz's foundry in Ohio. The mold itself was heated and placed into a 55-gallon drum of sand, so the chances of molten metal escaping from the split in the two halves were reduced. The metal was poured at 3000 F and had minimal excess or flashing from the mating surface tolerances. However, due to a modeling error, the guide holes for the split mold were mirrored incorrectly and the mold became slightly misaligned during the casting process. This caused there to be slight flashing and misalignment on some of the blades. Once the metal was cooled it was removed from the sand mold, shown in Fig. 14, and prepped for the next stage of manufacture.

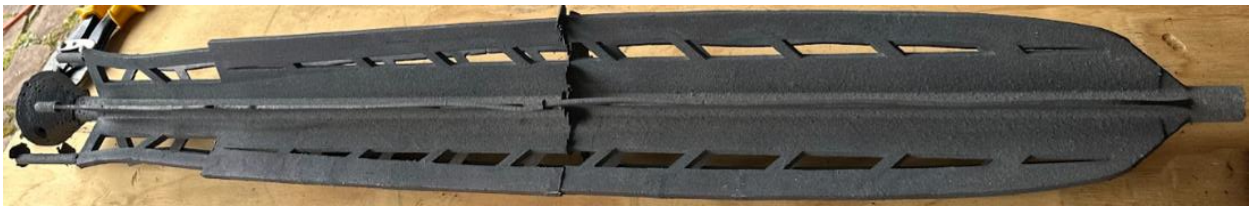

Figure 14. Cast structure removed from mold.

6.2 Cross guard and handle

Both the separate-component and single-component design were pursued; however, the single component design was ultimately chosen for the final blade for its simplicity, lighter weight, and aesthetics.

6.2.1 3D printing

The scaffolding for the separate component design was printed by LPBF, as seen in Fig. 15. This iteration of the design would require printing a separate mold structure to be able to cast the epoxy scales around the mounting pins, which would be structurally sound, but would significantly increase production time. The fit and finish process for this method would also cause heat soaking into the epoxy from grinding down the 316L pins, which could cause deterioration of the handle scales.

Figure 15. 3D printed scaffolding for separate-component design.

6.2.2 Sand casting

The single component design was fabricated by sand cast Al. The smallest details on the cross guard were removed since they would likely not transfer onto the cast part. To create the imprint for the sand casting, the model was 3D printed and smoothed with sandpaper and ethanol to remove any texture from the part to the cast structure. This smooth shape was then pressed into soft casting sand and cast in halves, as seen in Fig. 16. This product is what would eventually make it to the final sword as two halves can be fixed to the blade, and the assembly would be relatively complete, with minimal finishing work to carry out.

Figure 16. Single-component design after pouring in the sand mold.

7. Post processing

Once the mold was cast, the entire structure was heat treated to enhance the properties of the blade. Post processing involved solutionizing and aging the blade tree. This work was carried out while the blades were still attached to the tree in order to prevent warping that could occur during this process. Then, the swords were removed from the tree and various techniques were used to finish the cast blades into usable swords. The handles were also cast and finished, then attached to the finished blades to complete the assembly

7.1 Heat treatment

To achieve the ideal properties for a sword from CB7Cu-1, we require a heat treatment which maximizes hardness without negatively impacting ductility or strength. When designing the heat treatment, we consulted the ASM Handbook which provided mechanical properties for typical aging temperatures, shown in Fig. 17 [11].

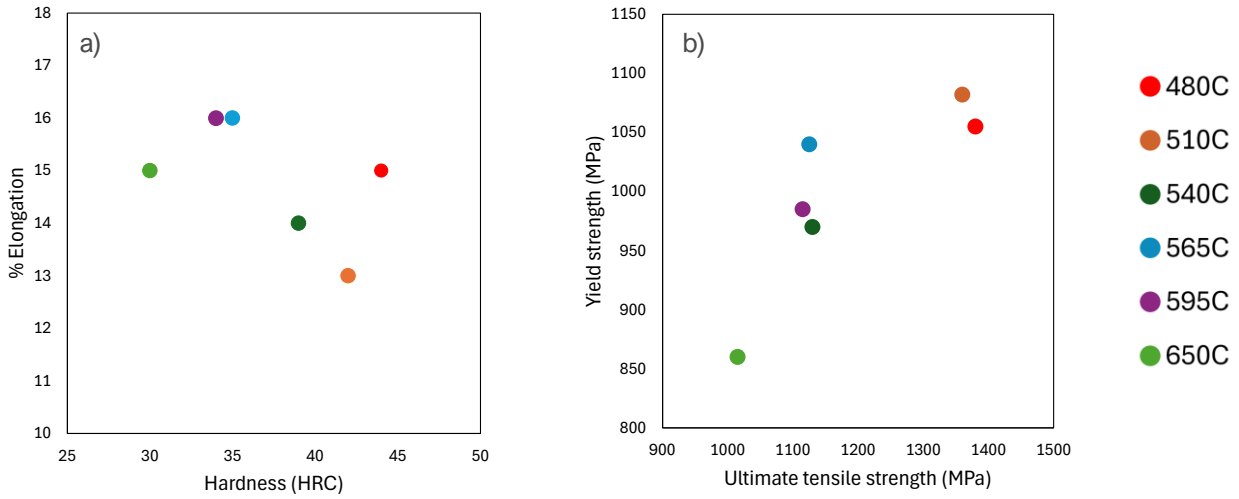

Figure 17. Mechanical properties resulting from 1 hour of aging for a range of temperatures: a) % elongation and hardness and b) yield strength and ultimate tensile strength. [11].

As seen in Fig. 17, for the same length of aging time, as aging temperature increases the hardness of the alloy decreases. The ductility, quantified by % elongation, remains mostly unaffected in a small range of 13% – 16% for all temperatures. Furthermore, at higher temperatures both yield strength and ultimate tensile strength are lower. Thus, the blade should be age hardened at a low temperature of 480C to obtain optimal mechanical properties.

With temperature determined, the next parameter we considered was aging time. Fig. 18 presents the mechanical properties obtained from age hardening at 480C for different lengths of time [11].

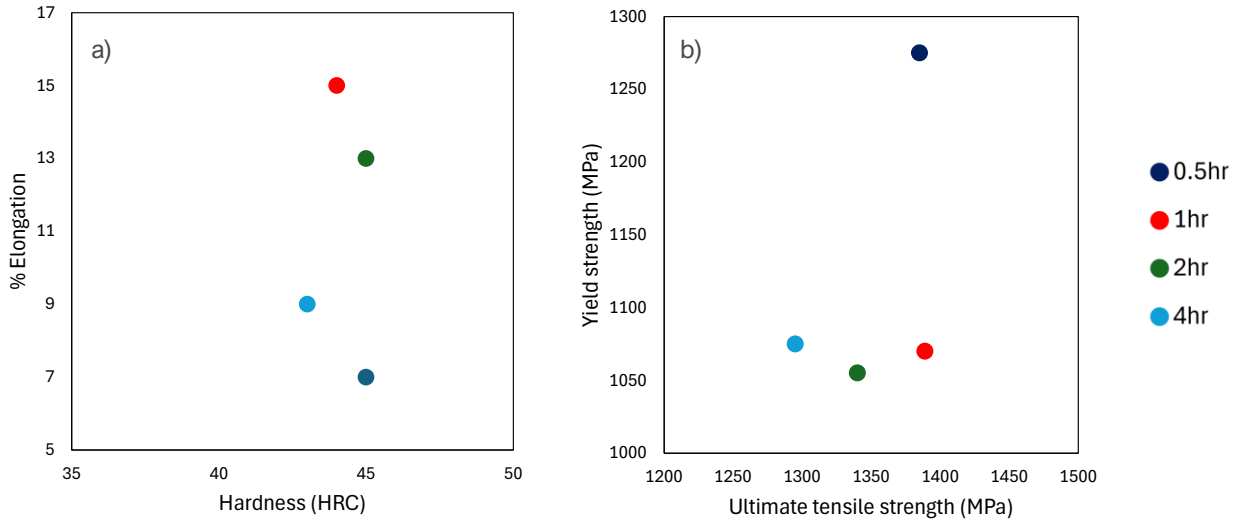

Figure 18. Mechanical properties resulting from aging at 480C for a range of times: a) % elongation and hardness and b) yield strength and ultimate tensile strength.

The mechanical properties most affected by aging time are ductility and ultimate tensile strength (UTS). Age hardening for 0.5 h shows a significant increase in yield strength, but a drastic decrease in ductility which is not optimal for a blade. All other aging times follow a general trend of

decreasing ductility and ultimate tensile strength as length of time increases. Thus, a shorter time of 1 hour at 480C will provide optimal hardness and yield strength without compromising the ultimate tensile strength or ductility. This leads us to the heat treatment shown in Fig. 19 that was applied to the casting.

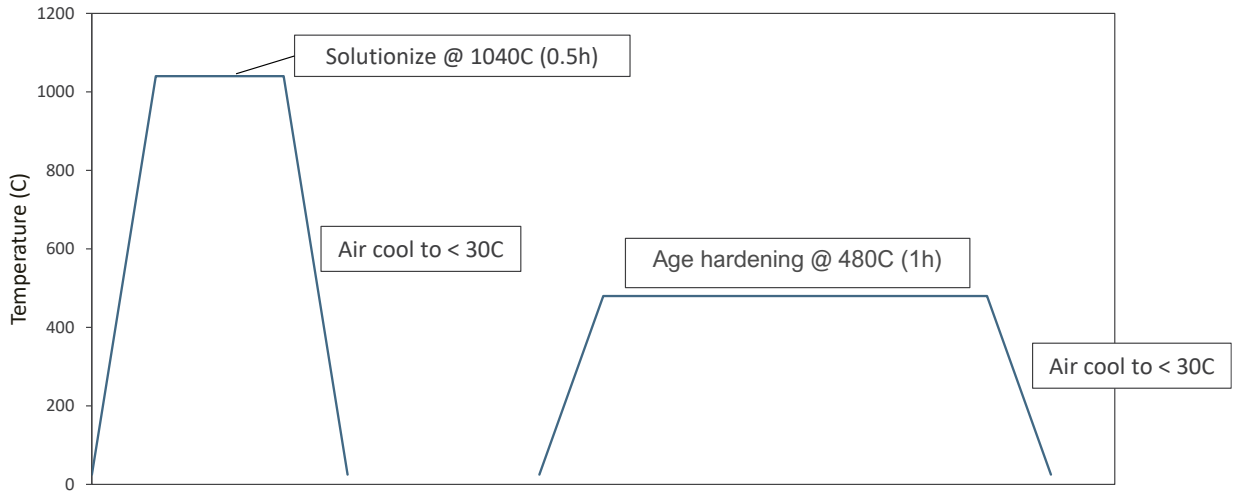

Figure 19. Heat treatment profile applied to the sword.

Preceding the age hardening step is a solutionization step which allows for the alloying metals to disperse evenly and create a homogeneous microstructure. The casting was then air quenched, age hardened, and air quenched again. This treatment ideally results in the mechanical properties described in Table 4 and enhances the alloy in a way that is optimized for the functions of a sword.

Table 4. Mechanical properties for aging at 480C for 1hr [11]

Hardness (HRC)	UTS (MPa)	σ_Y (MPa)	% Elongation
45	1380	1070	15

7.2 Machining, finishing, and assembly

Once cast both the blades and cross guard/handle component required machining to remove artifacts from the casting process. The blades were removed from the sprue using a plasma cutter and thinned to a spine thickness of 0.25 in. by a belt sander with a rough grit. A polished surface was achieved by wet sanding through progressively higher grits until the sword had a near mirror finish. After polishing, the blade was sharpened and an edge put on using progressive grit whetstones. The blade before and after these processes is shown in Fig. 20.

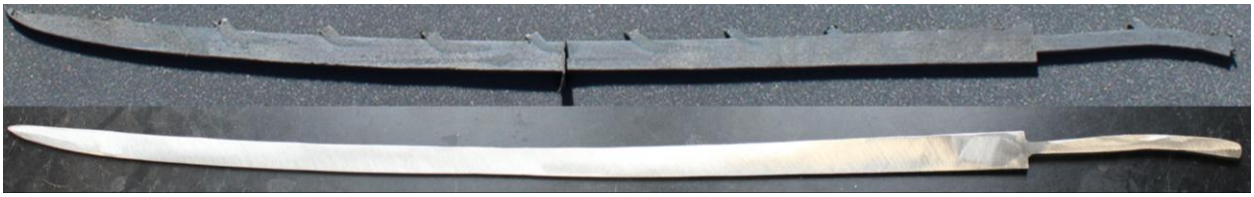

Figure 20. Blade before and after machining and finishing.

The handle and cross guard assembly was anodized orange, which electro-chemically created a protective oxide layer on the surface of the handle. To attach the handle, the tang of the blade was progressively shaped to fit the cavity of the cast handle assembly. When the handle was fitted onto the tang, three holes were drilled into the stacked handle-blade assembly to ensure concentricity for fitting pins. Epoxy was applied to the internal surfaces and clamped around the tang while three brass pins were pressed in to stabilize the interface. Finally, the exposed pins had to be removed using a small abrasive cutting disc, seen in Fig. 21, and were peened down flush to the grip for a smooth hold.

Figure 21. Brass pins being removed from the handle.

8. Analysis

To investigate the microstructure of the blade and the efficacy of our devised heat treatment, we took samples from the cast structure in the as-cast (AC) and heat-treated (HT) state. These samples were then tested for hardness and ran through a series of characterization techniques including scanning electron microscopy (SEM), energy dispersive spectroscopy (EDS), and X-ray diffraction (XRD).

8.1 Hardness

The hardness of the samples was evaluated using the Rockwell C method. Ten locations across each sample surface were taken and we consider the average of these measurements to be representative of the bulk hardness. The average hardness values obtained were 39.8 HRC for AC and 41.4 for HT. This value is lower than expected, and not in the range of suitable hardness for a blade.

To remedy this, we explored multiple different kinds of surface treatments including carburizing and nitriding. These methods would drastically increase the surface hardness of the blade while maintaining a ductile core [12]. This improvement is not without risk though as these methods can introduce brittle surface layers and decrease corrosion resistance [13]. Under advisement from Scott Roberts, a representative of Bodycote, we were recommended Kolsterising as a promising solution that can provide the benefits of a typical nitriding or carburizing while avoiding the common disadvantages. Unfortunately, due to timeline issues we were unable to apply this treatment to our blade.

8.2 Alloy verification

We obtained images of the microstructure using SEM and performed EDS on both AC and HT samples. The AC microstructures are shown in Figs. 22 a and b, while the HT microstructures are shown in Figs. 22 c and d. We performed EDS spot scans in two areas, shown in Fig 22a, to identify the composition of the black region and its surroundings. The black region is 40.93 wt% Ti and 19.08 wt% N. These elemental weight compositions led us to conclude that the sword has TiN precipitates. The composition of Spot 2 was measured as a comparison point, and results are within the range for CB7Cu-1 as described in Table 5. Region scans were done on Figs. 22 b and c to obtain a more representative composition of the samples. No amount of Ti nor N was measured, and Fe and Cr are back to expected levels for both AC and HT. The compositions of these region scans are summarized in Table 5 and we conclude that the elemental composition of the samples are withing textbook specifications of CB7Cu-1 and the heat treatment causes little to no change in composition.

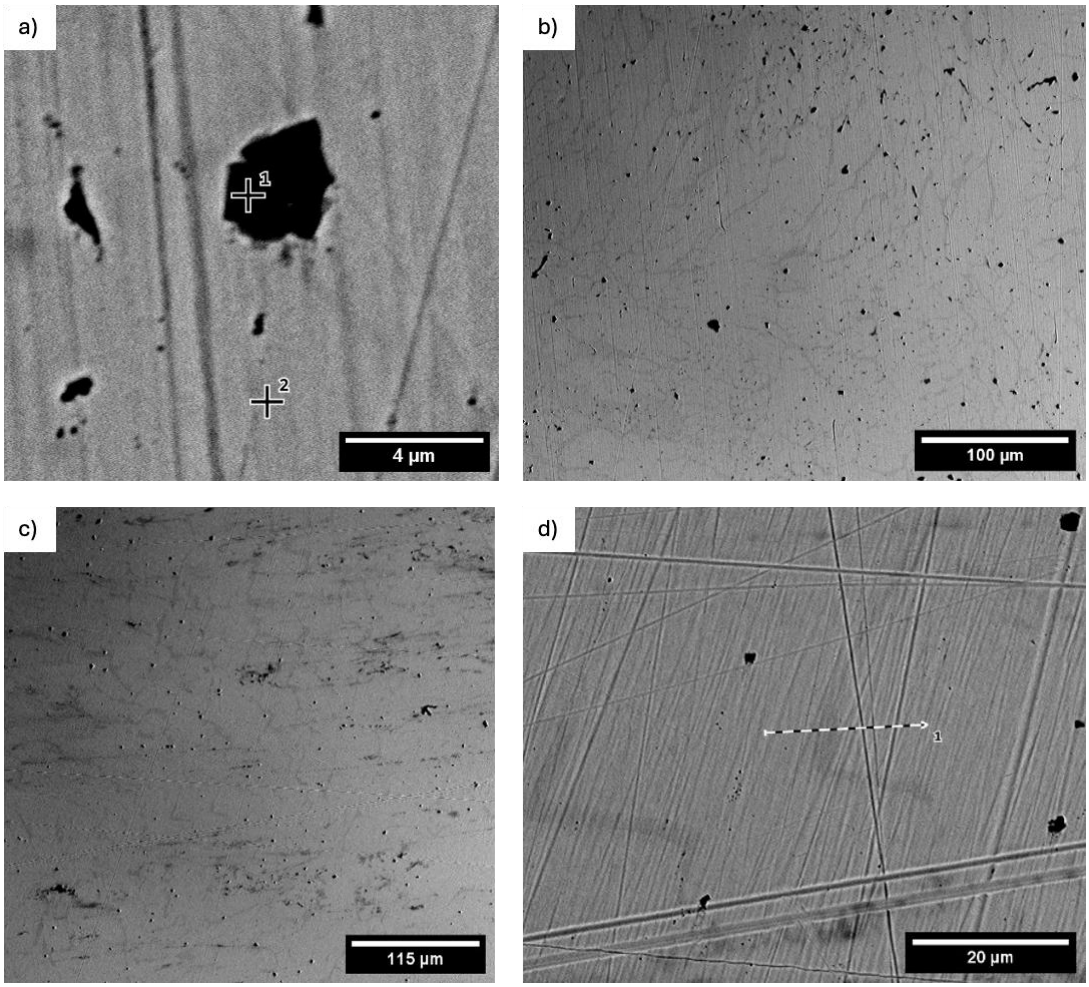

Figure 22. Micrographs of a-b) AC and c-d) HT CB7Cu-1 samples. a) and d) show EDS scan locations, and b-c) show representative sample surfaces.

Table 5. Elemental compositions in weight percent

	Fe	Cr	Cu	Ni	Mn	Si	Ti	N	Al
Textbook [14]	73.0	15.0-17.5	3.00-5.00	3.00-5.00	1.00	1.00	0.00	0.00	0.00
Spot 1	27.8	7.56	1.23	0.87	0.00	0.64	40.9	19.1	1.85
Spot 2	75.8	14.9	3.85	3.07	0.00	2.42	0.00	0.00	0.00
Region 1	75.3	15.3	3.80	3.30	0.00	2.25	0.00	0.00	0.00
Region 2	75.3	15.6	3.88	3.27	0.00	1.92	0.00	0.00	0.00
Line	74.8	15.2	3.71	3.46	0.88	1.90	0.00	0.00	0.00

Fig. 22d is a micrograph of our heat-treated sample that we performed EDS on in the form of a line scan, the composition of which is displayd in Table 5. In this figure, a dark gray region in the shape of an “L” can be seen which is a Cr vein. This is shown in Fig. 23 by a spike in the Cr line and a drop in the Ni and Cu lines. The spike occurs where the line scan touches the dark-gray lines in the micrograph. This led us to conclude that the dark-gray veins observed are Cr rich.

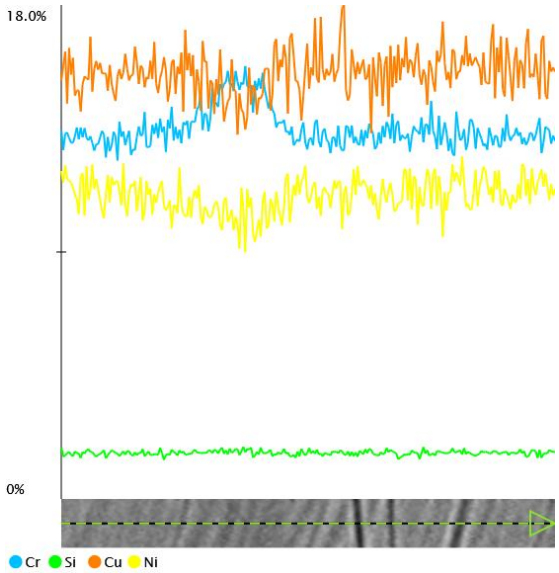

Figure 23. EDS elemental graphs of line scan.

To further verify the composition of our alloy, we performed EDS mapping, a technique that identifies elemental composition across an area of the sample and assigns colors to elements. The compositions found through this technique matched those found in the spot scans outlined above. Figure 24 shows these maps for the AC and HT samples. The AC sample map shows unevenly distributed carbon and identifies nitrides. The HT sample map shows that carbon was able to diffuse more evenly during heat treatment, but nitrides remain.

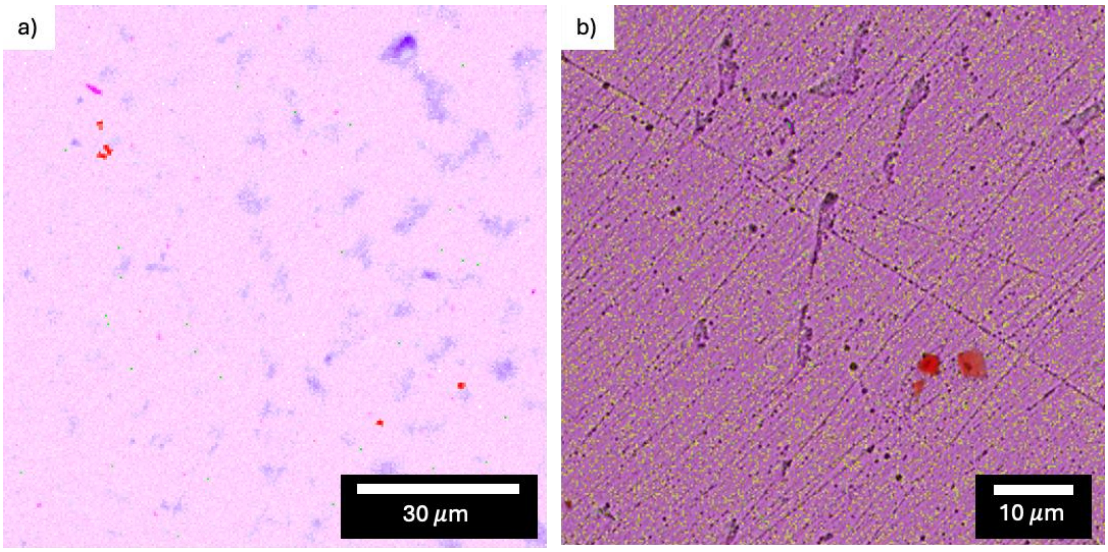

Figure 24. EDS maps of a) as-cast and b) heat-treated samples. Purple regions highlight areas rich in carbon; red regions highlight nitrogen.

8.3 Phase identification

To further understand the microstructure of the blade, we employed XRD to identify and quantify the phases of Fe present in both AC and HT samples. The resulting diffraction patterns are shown in Fig. 25.

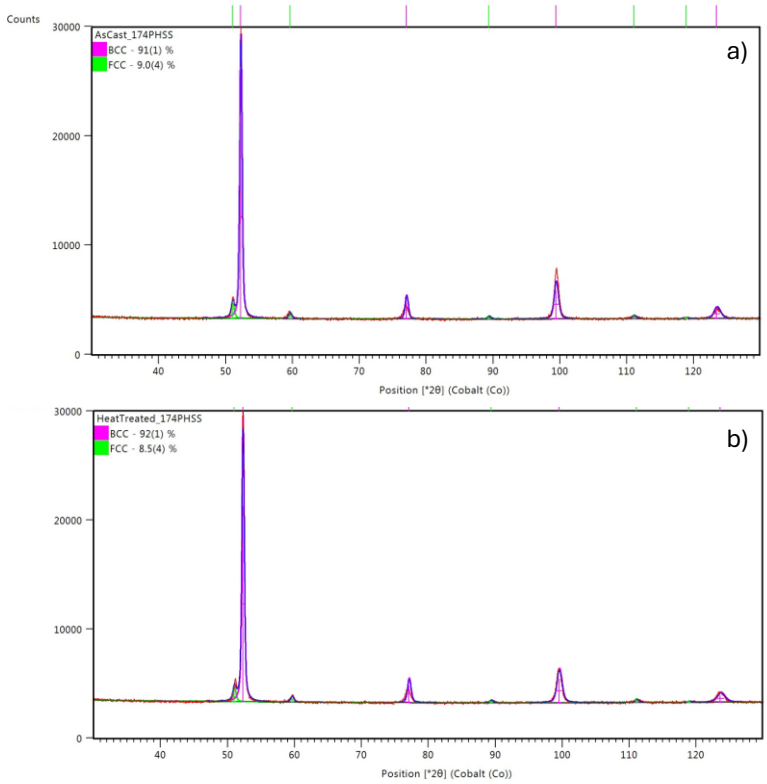

Figure 25. Diffraction patterns of a) AC and b) HT.

There is not much difference between the samples with both AC and HT samples composed of 91% BCC ferrite and 9% FCC austenite. Because the composition of the samples is nearly identical, yet the hardness differs, we can confirm that the mechanism behind the increase in hardness is precipitate growth rather than a decrease in retained austenite. It is of note that some fraction of the ferrite detected is martensite that is difficult to differentiate from ferrite using XRD.

9. Challenges

Team Sword Washington had to work through a few challenges during the sword-making process. These challenges included timeline issues, blade warpage, design issues, handle casting, and finishing touches. Even considering these challenges, we were able to push through and utilize our engineering skills to complete the sword and turn it in on time.

9.1 Timeline

Timing was our biggest challenge to overcome. The casting of the sword, considering the length and material, was not something that we were able to take on ourselves. This portion was outsourced, and with outsourcing comes some degree of release of control. Before the sword could be cast, we had to have the mold made, and before the mold could be made, we had to design it. Designing the mold took much of the time, and then casting the swords took up the remaining time. Initially, we were going to perform a surface treatment on the selected sword, but due to these time challenges, we were unable to complete the treatment. Because of some longer-than-expected shipping times, we received the sword with only one day before shipping to get it surface treated. Before surface treatment, the blade had to have an edge so that we would not grind off the treatment when sharpening. Ultimately, we could not finish grinding and get an edge on the blade in time to get it surface treated.

9.2 Blade-casting issues

The 6 blades were cast concurrently, as discussed above, and this had an 83% success rate. The failures in the cast are shown in Fig. 26a. One of the blades had a cold-shutting fault, seen in Fig. 26b and was deemed not available to use. (Another blade became highly warped after enduring the heat treatment process. This left us with the thickest blade to grind down to the final thickness desired of .250 inches. Another casting fault that occurred was a slight misalignment of the molds, shown in Fig. 26b. Due to a modeling error the alignment pins in the mold did not line up; this allowed the mold to slightly shift and resulted in some misaligned casts. These swords had no casting flow fault but instead endured a mold-alignment fault. Considering this, we deemed the ending success rate of the casting to be 50% as we did not count the warping after heat treatment.

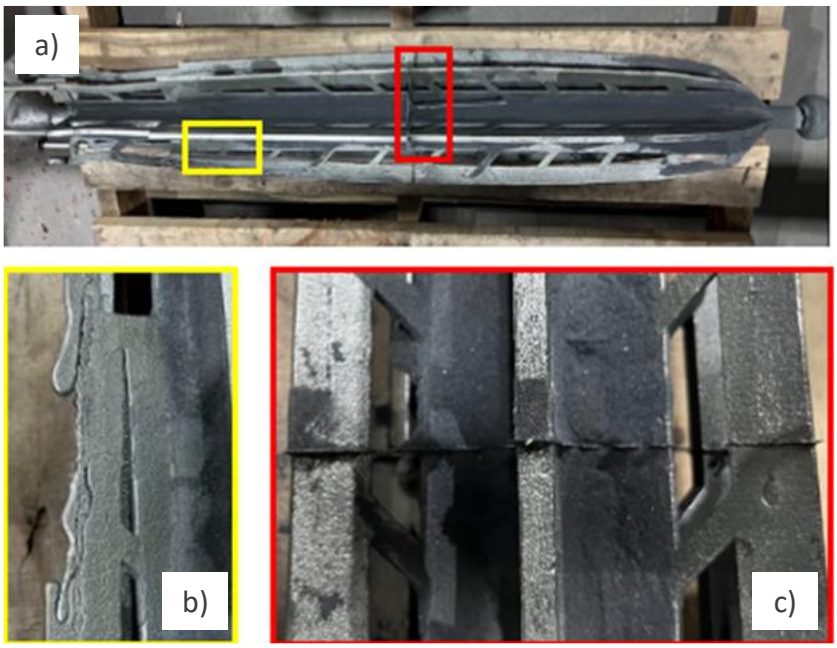

Figure 26. Casting failures seen a) on the whole cast structure, b) on the thinnest blade, and c) the misalignment.

9.3 Handle casting and anodizing

Team Sword Washington's replica sword contains a sand-mold-cast handle made from Al. This cast was performed in house and was completed on the second attempt. The first attempt was deemed a failure due to the sprue not being large enough to let the aluminum flow into the imprints. We fixed this issue by increasing the sprue diameter and adding more vents to allow the molten Al to flow fully into the cavities. Casting number two was deemed a high-quality, resounding success. After removing the handles from the sand mold, only a couple of hours of hand work was required to finish them into net shape.

The handles were also anodized, shown in Fig. 27, and with this came more issues. We taped off sections of the handle and applied paint to the areas we did not want to anodize. Unfortunately, the sulfuric acid dissolved the paint, and this method failed. The whole handle became orange after becoming electro-chemically plated. Because of this, more hand finishing had to be completed in order to remove the anodized layer from the desired sections of the handle.

Figure 27. Anodizing of the cross guard-handle assembly.

9.4 Finishing touches

One challenge of note was the final fitting of the handle onto the sword. The team decided to go with the original pin-and-epoxy style of mounting the handle onto the tang. This method requires precision drilling, but the holes we drilled through the handle pieces and the tang did not line up perfectly. Because of this, we were unable to use all three pins in the handle. Only the front and rear pins are through pins; the middle pin is not a through pin. With more time, this could have been resolved, but considering the detriment to structural integrity an additional hole would cause, it was decided to carry on without it.

10. Final results

After much grinding, polishing, and gluing the final sword was completed. It differs from the historical model with regards to the color of the handle, and the design of the centerpiece in the cross guard. All other dimensions of the blade were kept as close to the historical reference as possible. The blade had a final length of 30 inches and weighed ~ 650 grams as seen in Fig. 28.

Figure 28. The final assembled blade.

Acknowledgements

Throughout the entire process, Team Sword Washington was fortunate enough to receive assistance at every step from multiple parties. First, we would like to thank our faculty advisor Dr. Dustin Gilmer for his help throughout this process, scientifically and logistically. Second, we would like to thank Dr. Hahn Choo for teaching us the material-selection and design process and for his high standards for scientific presentation; they have been invaluable in the preparation of this report. Third, we thank Dr. Jerry Egeland endlessly for his contributions throughout the fabrication of this sword. His guidance made the sword possible. Fourth, we thank Dr. Bradley Jared for allowing us to use his SLM printer and Caleb Campbell for managing the printing and putting up with our repeated requests to rush this process. Finally from our in-house collaborators, Team Sword Washington would like to thank Tim Free of the UT machine shop for his help with various odd jobs.

The team would like to thank John Cory of Magotteaux for sponsoring us. We also thank Rafael Perez for his help with CFD simulation and mold design.

Various other professionals across the metallurgical profession deserve our thanks. Thank you, Dr. Philip King of the University of Maine and Dave Rittmeyer of Matthews Additive Technologies for your help informing our mold design. Also, thank you, Dr. Steve Feldbauer of Penn State University and Scott Roberts of Bodycote for sharing your knowledge of heat treatment.

Finally, we would like to acknowledge the vital work of Elizabeth Voss, Robert Palko, Joshua Hackenberg, Sandi Ricotta, Adam Smith, and their colleagues at Andritz in casting our blades.

References

[1] SFSA. https://www.sfsa.org (accessed Mar. 17, 2025).

[2] George Washington's Mount Vernon, "Washington's swords," https://www.mountvernon.org/preservation/collections-holdings/washingtons-swords?utm_source=chatgpt.com (accessed Mar. 17, 2025).

[3] Smithsonian, "George Washington's battle sword and scabbard," https://www.si.edu/object/george-washingtons-battle-sword-and-scabbard%3Anmah_434865?utm_source=chatgpt.com (accessed Mar. 17, 2025).

[4] Pooley Sword, "The evolution of swords," https://pooleysword.com/the-evolution-of-swords (accessed Mar. 17, 2025).

[5] Q. Zhang, F. Liu, D. Wu, S. Qu, W. Liu, and Z. Chen, "A Comprehensive Understanding of Knife Cutting: Effects of Hardness, Blade Angle and the Micro-Geometry of Blade Edge on the Cutting Performance," *Materials,* vol. 16, no. 15, p. 5375, 2023. [Online]. Available: https://www.mdpi.com/1996-1944/16/15/5375.

[6] M. Ashby, *Materials Selection in Mechanical Design*, 4th ed. Burlington, MA: Butterworth-Heinemann, 2011.

[7] Ansys Granta EduPack Software, 2024.

[8] H. Nakagawa and T. Miyazaki, 1999. Effect of Retained Austenite on the Microstructure and Mechanical Properties of Martensitic Precipitation Hardening Stainless Steel. Journal of Materials Science 34, 3901-3908. https://doi.org/10.1023/A:1004626907367.

[9] M. Villa, F. B. Grumsen, F. Niessen, T. Dahmen, L. Cao, M. Reich, O. Kessler, X. Huang, and M. A. J. Somers, 2023. Aging 17-4 PH Martensitic Stainless Steel Prior to Hardening: Effects on Martensitic Transformation, Microstructure and Properties. Mtla. 32(2023), 101882. https://doi.org/10.1016/j.mtla.2023.101882.

[10] The Mount Vernon Ladies' Association. The Bailey Silver & Ivory Hilted Cuttoe. https://www.mountvernon.org/preservation/collections-holdings/washingtons-swords/the-bailey-silver-ivory-hilted-cuttoe.

[11] ASM International, 2009. ASM Handbook Revised Vol. 4: Heat Treating. ISBN-13: 978-0-87170-379-8.

[12] A.Kosmač: Surface Hardening of Stainless Steels, Second edition 2015, Materials and Applications Series, Volume 20, Euro Inox, ISBN 978-2-87997-395-1;

[13] B. Edenhofer, D. Joritz, M. Rink and K. Voges, "Carburizing of steels," in *Thermochemical Surface Engineering of Steels: Improving Materials Performance,* E. J. Mittemeijer and M. A. J. Somers, Elsevier Science and Technology, 2014, 485-553. [Online].

[14] AZO Materials, "Stainless steel - Grade 17-4 (UNS S17400)." https://www.azom.com/article.aspx?ArticleID=6778. Sept. 26, 2012.